

Role of AGNs in the Ultra-Luminous Infrared Galaxy phase since $z \sim 3$

Ming-Yi Lin^{1*}, Sébastien Foucaud¹ and Yasuhiro Hashimoto¹

¹*Department of Earth Sciences, National Taiwan Normal University, No.88, Tingzhou Road, Sec. 4, Taipei 11677, Taiwan (R.O.C.)*

Accepted 20XX Month Day. Received 20XX Month Day; in original form 2013 January 12

ABSTRACT

In order to understand the mutual influence between active galactic nuclei (AGN) and star formation during the evolution of galaxies, we investigate 142 galaxies detected in both X-ray and 70 μ m observations in the COSMOS (Cosmic Evolution Survey) field. All of our data are obtained from archive, X-ray point source catalogs from Chandra and XMM-Newton observation; far-infrared 70 μ m point source catalog from Spitzer-MIPS observation. Although the IRAC colors of our samples indicate the existence of star formation, the ratio of rest frame 2–10 keV luminosity to total infrared luminosity (8–1000 μ m) shows that AGN predominates the spectral energy distribution (SED). We identify obscured AGN in these 70 μ m luminous galaxies as characterized by a larger hardness ratio. The higher X-ray obscuration fraction indicates an extra contribution from the star formation in the host galaxy in addition to the usual AGN dusty torus. If AGN feedback occurs in their host galaxies, the star formation must be quenched and dust in host galaxy will be dispersed. However, our temperature fitting shows there is no significant dust temperature enhancement in far-infrared wavelength, suggesting the thermal radiative feedback is absent from the AGN to the galaxy.

Key words: galaxies: high-redshift – galaxies: active – infrared: galaxies – X-rays: galaxies.

1 INTRODUCTION

Both observational and theoretical evidences over the past decades strongly suggest the existence of supermassive black hole (SMBH) within the spherical bulge of galaxies. The tight connection between the SMBH mass and the bulge properties, such as bulge luminosity or stellar velocity dispersion, indicates a scenario of co-evolution for central black hole and its host galaxy (Kormendy & Richstone 1995; Magorrian et al. 1998). Galaxy merger is a plausible interpretation to explain the concomitant growth of black hole and host galaxy under the Λ CDM model (Treister et al. 2010). Such interpretation implies the mergers distort galaxy morphology and trigger the intense star formation, producing a large amount dust and molecular gas (Magdis et al. 2011). Meanwhile, interstellar medium (ISM) is also funneled onto the SMBH in the galactic nucleus and consequently triggers a phase of active galactic nuclei (AGNs), with its powerful electromagnetic radiation spanning from radio to gamma-ray. In the later galaxy evolution stage, the merger scenario implies that the radiation-pressure or kinematic-wind feedback from AGN may quench the star formation, disrupting the remnant gas and dust. At the same time, central AGN turns into an optically unobscured quasar, a class of luminous AGN. Final outcome in galaxy evolution is a red elliptical galaxy (Hopkins et al. 2008).

Sanders et al. (1988a) first proposed a connection between the Ultra Luminous Infrared Galaxies (ULIRGs; $L_{\text{IR}} \geq 10^{12} L_{\odot}$) and quasars as two successive snapshots of merger event between two gas-rich spiral galaxies. Indeed, from IRAS 1 Jy ULIRGs studies, the merger-ULIRG connection has been revealed by a large fraction of interacting galaxies at $z < 0.1$ (Borne et al. 2000; Cui et al. 2001; Veilleux et al. 2002). Besides, the merger fraction has been shown to increase as infrared luminosity raises, merging galaxy being prevalent population amongst ULIRGs to redshift ~ 1 (Shi et al. 2009). However at higher redshift ~ 2 , the merging galaxy fraction drops slightly and non-interacting disk galaxy fraction increases (Kartaltepe et al. 2012).

On the other hand, the merger-AGN connection is more difficult to observe. Although, in the local universe, optical luminous quasars are considered to be related to post-starburst merger stage (Canalizo & Stockton 2001; Bennert et al. 2008), at $1.5 < z < 2.5$, AGNs are more likely to occur inside of normal disk or bulge galaxy, instead of interacting systems, suggesting that secular processes (such as bars or nucleus rings) may trigger nuclear activity instead of major-mergers (Kocevski et al. 2012). The potential connection between ULIRGs and AGNs, is still under investigation, and the nature of underlying physical process responsible for such extreme far-infrared luminosity is in debate (Sanders & Mirabel 1996; Farrah et al. 2003).

In order to determine the exact role of the AGN in the overall galaxy evolution, it is essential to separate the AGN contribution from the normal star formation activity. To decouple two compo-

*E-mail: 699440083@ntnu.edu.tw

nents, we can use three distinct methods:

(i) *Specific emission lines ratio* - Fine structure radiation in optical and infrared wavelength are reliable tracers of excitation state of the ISM in galaxies. A classification based on two independent line ratios can help to segregate AGN and star-forming galaxies. For instance, investigating $[\text{OIII}]5007\text{\AA}/\text{H}\beta$ versus $[\text{NII}]6584\text{\AA}/\text{H}\alpha$ (Baldwin et al. 1981, BPT) diagram will lead to distinguish the photoionization, derived from normal HII regions, from power-law continuum generated by AGNs. Unfortunately, galaxies undergoing merger event suffer from dust obscuration in optical wavelength that limits the efficiency of such diagnostics.

By the advent of the infrared spectrometer (IRS) on the Spitzer telescope, additional emission lines were identified for AGN diagnostics in the mid-infrared, that are less sensitive to extinction. For example, the line ratio $[\text{O IV}]25.9\mu\text{m}/[\text{NeII}]12.8\mu\text{m}$ or $[\text{NeV}]14.3\mu\text{m}/[\text{NeII}]12.8\mu\text{m}$ is a reliable indicator to separate AGNs from star-forming galaxies (Armus 2006). The different transition lines of Polycyclic Aromatic Hydrocarbon (PAH) molecules are other reliable tracers, with weaker PAH emission corresponds to higher AGN contribution (Voit 1992; Veilleux et al. 2009);

(ii) *Continuum slope* - As the influence of the AGN becomes significant in the galaxy, the infrared spectral indexes start to be dominated by a power-law continuum at $\sim 10\mu\text{m}$ (Alonso-Herrero et al. 2006; Donley et al. 2007). For longer wavelengths, the mid-infrared to far-infrared ratio is a simple measure to quantify the relative contributions of AGNs and star-forming galaxies (Veilleux et al. 2009);

(iii) *Spectral energy distribution fitting* - With the development of deep multi-wavelength photometric surveys, panchromatic Spectral Energy Distribution (SED) studies are becoming increasingly popular. Theoretical or empirical templates are commonly used to fit the SED and determine the photometric redshifts of galaxies. Multi-component fitting, including the contribution from stars, dust, and AGNs is now possible thanks to very broad photometric coverage. In the case of heavily obscured AGNs, although star formation of host galaxy dominates the flux at most wavelengths, a bump in mid-infrared produced by the circumnuclear dust radiation, can be an indicator of an obscured AGN. Therefore, identifying hot dust component from the galaxy SED is a reliable way to determine the AGN contribution to total infrared luminosity (Mullaney et al. 2011; Pozzi et al. 2012).

Although the different methods may not agree completely on defining a pure sample (i.e. pure-AGN or pure starburst galaxy), they all provide evidences that, for the major part of the samples, AGN and star formation occur concomitantly. Rather than just pursuing the intrinsic AGN contribution fraction on the total infrared luminosity, what is essential here is to understand the mutual influence on the properties of AGNs and hosts star-forming galaxies.

The SEDs of Luminous Infrared Galaxies (LIRGs; $10^{11} L_{\odot} \leq L_{\text{IR}} < 10^{12} L_{\odot}$) and ULIRGs are peaked in the range of 40-200 μm (Sanders & Mirabel 1996). In fact, the 70 μm Spitzer band is ideal to unambiguously trace star-forming galaxies as it is little affected by PAH emissions, silicate absorption, and stellar flux. Central AGNs are usually identified by their strong X-ray continuum emission. Indeed, high energy X-ray photons emitted by hot corona of accretion disk (e.g., Haardt & Maraschi 1993) around the central black-hole are usually little absorbed by dust and gas from host galaxies, compared to lower energy UV-photons. One noticeable exception are compton thick objects ($N_H \geq 10^{24} \text{ cm}^{-2}$) for which even hard X-ray photons are absorbed.

Several studies have investigated the nature of the 70 μm

galaxy population. Patel et al. (2011) lead a spectroscopic follow-up in optical wavelength of 70 μm galaxies selected from the Spitzer Wide-area Infrared Extragalactic Legacy Survey. Their results suggest that the most of the IR photons are powered by star formation, while contribution from AGN dusty torus emission are negligible for the non-QSO-dominated samples. From the SED study of 61 70 μm selected galaxies from the 0.5 deg² wide Extended Groth Strip (EGS) field, Symeonidis et al. (2010) concluded that, even in the presence of powerful hard X-ray emission originated from AGNs, dust emission templates are required to explain the observed strong far-infrared luminosity. To reveal a potential starburst-AGN connection, Trichas et al. (2009) used a statistical K-S test (Kolmogorov-Smirnov test) to assess differences in hardness ratio between X-ray detected 70 μm galaxies and the whole X-ray population. However, shallow observations in both far-infrared and X-ray lead to a less significant probability of the K-S test, interpreted as low hydrogen column density (N_H) in the nearby SMBH. This result is in contrast to current galaxy formation scenario (Hopkins et al. 2008).

In this paper, we aim to dissect the role of AGN in the (ultra)infrared luminous phase of galaxy evolution. We extracted the X-ray detected sub-sample from unconfused 70 μm catalog. Our main 70 μm galaxy catalog was published by Kartaltepe et al. (2010), including total infrared luminosity, multi-wavelength photometry and redshift. We describe the data used for this work in section 2. As we are interested in physical property of AGN and far-infrared selected host galaxy, we cross-match X-ray and 70 μm datasets. In section 3, we depict our matching method as well as the methods used to estimate and calibrate different physical parameter measurements. We present our results in section 4, and then conduct a detailed discussions in section 5. Throughout this paper, we adopt a fiducial cosmological model with the following parameters: $H_0 = 70 \text{ km s}^{-1} \text{ Mpc}^{-1}$, and $\Omega_M = 0.3$, $\Omega_{\Lambda} = 0.7$. Unless otherwise stated, all magnitudes in this paper are in the Vega system.

2 DATA

The Cosmic Evolution Survey (COSMOS) is the largest treasury program using Hubble Space Telescope, imaging a $\sim 2 \text{ deg}^2$ -wide equatorial field in the optical F814W filter (approximately corresponds to I band) with the Advanced Camera for Surveys (ACS) instrument (Scoville et al. 2007a,b; Koekemoer et al. 2007). Several large follow-up campaigns using ground-based and space-based telescopes produced the deepest comprehensive photometric and spectroscopic dataset across a whole spectrum (Capak et al. 2007; Hasinger et al. 2007; Sanders et al. 2007; Scott et al. 2008)¹. Our initial catalog is a 70 μm catalog extracted by Kartaltepe et al. (2010), who have publicly released their measured total infrared luminosity, redshifts, and multi-wavelength photometry. Here, we will give a brief description of our infrared and X-ray datasets.

2.1 Spitzer-COSMOS

Spitzer-COSMOS (S-COSMOS) is a Legacy program designed to cover the COSMOS field with deep Spitzer observations in IRAC four bands (i.e. 3.6, 4.5, 5.8, and 8.0 μm) and MIPS three bands

¹ c.f. the COSMOS Special Issue of the Astrophysical Journal Supplement Series, in September, 2007.

(i.e. 24, 70, and 160 μm). The initial Cycle 2 program conducted in 2006 consists of a deep IRAC survey, a shallow MIPS survey, and a small deep MIPS survey. The total integration time of the deep IRAC survey is 166 hours, reaching 5σ sensitivities of 0.9, 1.7, 11.3, and 14.6 μJy , in 3.6, 4.5, 5.8, and 8.0 μm band, respectively (Sanders et al. 2007). A complementary MIPS deep observation of 450 hours has been conducted in Cycle 3, ensuring accurate 70 and 160 μm flux density measurements. The median exposure times were $\sim 3400\text{s}$, 1350s, and 270s for 24 μm , 70 μm , and 160 μm band, respectively, corresponding to 5σ depths of ~ 0.08 , 8.5, and 65 mJy (Le Floch et al. 2009; Frayer et al. 2009; Kartaltepe et al. 2010).

2.2 X-ray dataset: XMM-Newton & Chandra

The COSMOS field has been covered with observation from both XMM-Newton (XMM) and Chandra telescopes.

A 2 deg^2 contiguous survey has been conducted with XMM to reach medium depth (~ 60 ks). COSMOS X-ray catalog made by XMM observation (XMM-COSMOS) provides three different energy bands. Base on the logN-logS relationship, the flux limit of 0.5-2 keV (soft band), 2-10 keV (hard band), and 5-10 keV (full band) drop to 7.2×10^{-16} ergs $\text{cm}^{-2} \text{s}^{-1}$, 4.0×10^{-15} ergs $\text{cm}^{-2} \text{s}^{-1}$, and 9.7×10^{-15} ergs $\text{cm}^{-2} \text{s}^{-1}$, respectively (Hasinger et al. 2007; Cappelluti et al. 2009). In total, 1887 point-like sources were identified in the XMM-COSMOS survey. Brusa et al. (2010) has released a cross matched catalog between these sources and optical counterparts (I band, catalog of Capak et al. (2007)), providing redshifts (spectroscopic and photometric), UV to 24 μm photometry, and hardness ratio.

The Chandra-COSMOS (C-COSMOS) Survey images a ~ 0.9 deg^2 field in the central part of the original COSMOS field, with the effective exposure time ~ 160 ks in center 0.5 deg^2 and ~ 80 ks in outer 0.4 deg^2 . C-COSMOS catalog provides three different energy bands, 0.5-2 keV (soft band), 2-7 keV (hard band), and 0.5-7 keV (full band), with corresponding flux limits of 1.9×10^{-16} ergs $\text{cm}^{-2} \text{s}^{-1}$, 7.3×10^{-16} ergs $\text{cm}^{-2} \text{s}^{-1}$, and 5.7×10^{-16} ergs $\text{cm}^{-2} \text{s}^{-1}$, respectively. In total, 1761 point-like sources have been extracted in the in C-COSMOS field (Elvis et al. 2009).

In this paper, we combine observations from XMM and Chandra, taking advantage of the wider observational field of XMM-COSMOS and the deeper observational depth of C-COSMOS, to maximize the total number of X-ray point source counterparts of our 70 μm selected galaxy sample.

3 METHOD

3.1 Matched X-ray and far-infrared point source catalog

The spatial resolution of the Spitzer Telescope at 70 μm is around $18''$, much larger than the spatial resolution of XMM or Chandra X-ray observatory. Therefore, it is crucial to accurately detect the position of the 70 μm galaxies. Kartaltepe et al. (2010) have identified the optical or near-IR counterpart of 70 μm selected galaxies. We took advantage of the Altas resource from IRSA/COSMOS archive² to match the optically identified counterpart of 70 μm selected sources with the XMM and Chandra point source catalogs, separately. We identified 108 and 92 70 μm counterparts by matching with XMM and Chandra using searching radii of $3''$ and $1''$,

respectively. The median angular distances between the position of the X-ray source and the position of optical/near-IR identified counterpart of our 70 μm -selected galaxies are $0.9''$ and $0.3''$ for the XMM and Chandra point source catalogs, respectively. Fifty-eight sources were identified in both X-ray catalogs, and a total number of one hundred and forty-two galaxies have been identified to have both 70 μm and X-ray measurements in the COSMOS field. We will refer to this sample as "70 μm /X-ray" galaxy catalog in the remaining part of this article. From the same datasets, Kartaltepe et al. (2010) identified 154 X-ray detected 70 μm galaxies. The 12 extra objects compared to our own matching catalog are originated from a slightly less strict matching criterion. These additional sources are more distant from the 70 μm source position. The number of sources from our different catalogs and matched catalogs are summarized in Table 1.

3.2 Redshift determination

Several spectroscopic surveys were conducted to measure the redshifts of galaxies in the COSMOS field. The most extensive survey on this field is the zCOSMOS survey (Lilly et al. 2007), a deep spectroscopic survey conducted with the VLT-VIMOS multi-object spectrograph to study the evolution of faint/obscured galaxies through direct analysis of their emission lines. Although the observations enable us to probe properties of faint objects, only the central 1 deg^2 is covered by zCOSMOS. Forty-nine of our 70 μm /X-ray galaxies had their redshifts confirmed spectroscopically by zCOSMOS. Observations using other facilities have been conducted on this field providing precise redshifts for fifty-three additional 70 μm /X-ray galaxies (Abazajian et al. 2009; Trump et al. 2007; Kartaltepe et al. 2010; Prescott et al. 2006). In total 102/142 (71.8%) galaxies with X-ray and 70 μm detection have spectroscopic redshift. Table 2 summarize the origin and number of our targets with spectroscopic redshifts.

For the remaining galaxies, we used the photometric redshift catalogs built for both non-AGN sources and XMM-selected sources (Ilbert et al. 2009; Salvato et al. 2009), using the public available software Le PHARE³ (Arnouts et al. 1999; Ilbert et al. 2006). The 70 μm /X-ray galaxies which do not have spectroscopic redshift have been assigned a photometric redshift (40 out of 142 - 28.2%).

The photometric and spectroscopic redshifts of 70 μm /X-ray galaxies follow the overall 70 μm galaxy relation with a scatter of $0.02 \times (1+z)$ (Kartaltepe et al. 2010). Bright sources have usually been assigned a spectroscopic redshift, with small error, while faint sources have been assigned a photometric redshift with larger error. Fortunately, even though these two different methods for redshift measurement have different error sizes, the infrared and X-ray luminosity distribution inferred both by spectroscopically and photometrically determined redshifts have the same median value. Therefore, we conclude the difference in redshift measurements does not induce any systematic bias.

Figure 1 shows the redshift distribution in different infrared luminosity intervals, star-forming galaxies (SFGs; $L_{\text{IR}} < 10^{11} L_{\odot}$) with median $z \sim 0.168$, luminous infrared galaxies (LIRGs; $10^{11} L_{\odot} \leq L_{\text{IR}} < 10^{12} L_{\odot}$) with median $z \sim 0.518$, and ultra-luminous infrared galaxies (ULIRG; $L_{\text{IR}} \geq 10^{12} L_{\odot}$) with median $z \sim 1.268$ (for more details on the computation of L_{IR} please see section 3.3).

² NASA/IPAC infrared service archive of COSMOS project. <http://irsa.ipac.caltech.edu/data/COSMOS>

³ <http://www.cfht.hawaii.edu/~arnouts/LEPHARE>

Table 1. Samples properties and matching results

Catalog	Area ^(a) in deg ²	Flux limits ^(b) in mJy ^(†) or 10^{-16} ergs cm ⁻² s ⁻¹ ^(‡)	N_S ^(c)	$N_{70\mu\text{m}}$ ^(d)	References ^(e)
Spitzer-COSMOS (S-COSMOS) 70 μm galaxies catalog	2.47	8.5 ^(†) (5 σ)	1503	1503	Frazer et al. (2009) & Kartaltepe et al. (2010)
XMM-COSMOS Point source catalog	2.13	7.2 ^(‡) (Soft band) 40 ^(‡) (Hard band) 97 ^(‡) (Full band)	1886	108	Cappelluti et al. (2009) & Brusa et al. (2010)
Chandra-COSMOS (C-COSMOS) Point source catalog	0.50 (Deep) 0.40 (Shallow)	1.9 ^(‡) (Soft band) 7.3 ^(‡) (Hard band) 5.7 ^(‡) (Full band)	1761	92	Elvis et al. (2009)
XMM- & Chandra-COSMOS concatenated catalog ^(f)	—	—	2821	142	This work

^(a)Effective area covered by the survey; ^(b) Flux limit of the catalog; ^(c)Total number of sources; ^(d)Number of sources cross-matched with the 70 μm catalog; ^(e)References describing the catalog; ^(f)Catalog concatenated from XMM- and Chandra-catalogs; sources matched between the two catalogs are not duplicated; the cross-match between this catalog and the 70 μm catalog constitute our primary “70 μm /X-ray” catalog.

Table 2. Confirmed spectroscopic redshift sample

Telescope	Instrument	$N^{(a)}$	Reference
ESO-VLT	VIMOS	49	zCOSMOS Lilly et al. (2007)
Magellan	IMACS	26	Trump et al. (2007)
Sloan	SDSS	15	Abazajian et al. (2009)
Keck II	DEIMOS	11	Kartaltepe et al. (2010)
MMT	Hectospec	1	Prescott et al. (2006)

^(a)Number of 70 μm /X-ray sources with spectroscopic redshift.

3.3 Total infrared luminosity

Kartaltepe et al. (2010) estimated the total infrared luminosity (L_{IR}) for all 70 μm -selected galaxies, by fitting a SED with a χ^2 -minimization method using Le PHARE³ and integrating the luminosity over the 8-1000 μm wavelength range.

The current public COSMOS 70 μm -catalog from Kartaltepe et al. (2010) has been constructed carefully taking into account the possible AGN contamination: they only used 24, 70, and 160 μm photometric data. However, this catalog suffers incompleteness in the 160 μm band, and lacks any direct photometric observation in Rayleigh-Jeans part of the SED. Kartaltepe et al. (2010) assessed that measurements of L_{IR} without 160 μm data are underestimated by 0.2 dex compared to measurements with 160 μm data. Despite these caveats, we estimate that this catalog is robust enough for our study, as the galaxies without 160 μm photometry are equally spread between the samples with or without X-ray detected 70 μm galaxies.

We divided our 70 μm /X-ray galaxy sample into three distinct classes according to their total infrared luminosity as star-forming galaxy (SF), luminous infrared galaxy (LIRG), and ultra-luminous infrared galaxy (ULIRG) with $L_{\text{IR}} < 10^{11} L_{\odot}$, $10^{11} L_{\odot} \leq L_{\text{IR}} < 10^{12} L_{\odot}$, and $L_{\text{IR}} \geq 10^{12} L_{\odot}$, respectively. The redshift distributions of our three classes are represented in Figure 1.

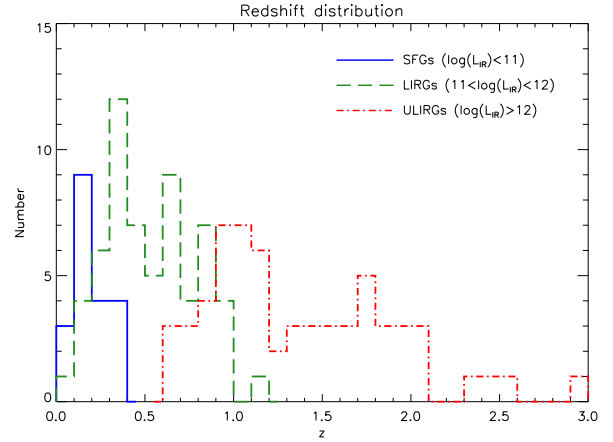


Figure 1. The redshift distribution of 70 μm /X-ray galaxies. We divided our total sample into three distinct classes selected according to their total infrared luminosity : star-forming galaxies (SFGs; $L_{\text{IR}} < 10^{11} L_{\odot}$; blue solid line) at a median redshift of $z \sim 0.168$, luminous infrared galaxies (LIRGs; $10^{11} L_{\odot} \leq L_{\text{IR}} < 10^{12} L_{\odot}$; green dash line) at $z \sim 0.518$ and ultra-luminous infrared galaxies (ULIRG; $L_{\text{IR}} \geq 10^{12} L_{\odot}$; red dash-dot line) at $z \sim 1.268$.

3.4 Estimating dust temperature of host galaxy

In the local universe, the far-infrared luminosity is assumed to be driven by the emission from dust grains contained in the galaxy. Far-infrared photometry becomes a critical indicator to reveal the dust properties of the galaxy. Owing to the deep Spitzer observations, we identified 463 (463 out of 1503; 31%) 70 μm sources, amongst which 52 (52 out of 142; 37%) of our 70 μm /X-ray galaxies, with 160 μm counterparts. Most (89%) of 160 μm detected sources have a single matched 70 μm source inside MIPS error circle. While for the remaining sources with multiple 70 μm counterparts, Kartaltepe et al. (2010) assigned the brighter one as counterpart of the 160 μm source.

Using the 70 μm and 160 μm fluxes, we adjusted a single temperature model represented by a modified blackbody radiation, as

following:

$$F_\nu = \nu^\beta B_\nu(\nu, T) \quad (1)$$

with a fixed emissivity $\beta \sim 1.5$ (Clements et al. 2010)

We restrict the temperature range from 5K to 205K, typical for dust temperature of submillimeter galaxies (SMGs) and ULIRG (Chapman et al. 2005; Kovács et al. 2006; Yang et al. 2007; Casey et al. 2009). Models are convolved with Spitzer-MIPS filter response, and the best temperature is fitted using a minimum χ^2 method:

$$\chi^2 = \sum_i \left[\frac{F_{obs,i} - n F_{model,i}}{\sigma_i} \right]^2 \quad (2)$$

where i refers to $70\mu\text{m}$ and $160\mu\text{m}$ flux densities and n is the normalization factor to the $160\mu\text{m}$ flux density.

To ensure an accurate estimation of the dust temperature in high-redshift galaxies, we exclude the $24\mu\text{m}$ fluxes from our SED fitting, mainly because of:

(i) Contamination of the flux in the $5\text{--}30\mu\text{m}$ range by emissions from the AGN dust torus or alternatively a potential hot dust component (Brand et al. 2006; Pozzi et al. 2012), (ii) Presence of several Polycyclic Aromatic Hydrocarbon (PAH) transition lines (e.g. 6.2 , 7.7 , and $11.3\mu\text{m}$ emission lines) entering the $24\mu\text{m}$ band at $z \sim 1$, (iii) Presence of strong silicate absorption feature at $9.7\mu\text{m}$, which is strongly correlated with the optical depth; in particular in the case of ULIRGs, presence of large amount of dust grains causes the distinct absorption features (Levenson et al. 2007).

3.5 Correction of X-ray properties

With the help of combining both XMM and Chandra X-ray catalogs, we extend our total sample of $70\mu\text{m}$ /X-ray galaxies to 142 sources, of which 58 are listed in both X-ray catalogs. The count rates for these sources have been converted into $0.5 - 2\text{keV}$ (soft band) and $2 - 10\text{keV}$ (hard band) flux density for both XMM and Chandra observations by assuming a power-law spectrum (Cappelluti et al. 2009; Elvis et al. 2009). For the 58 sources with overlapping detections between the two catalogs, we confirmed that both fluxes from XMM and Chandra are consistent, with a 1σ error within 0.219 in log space.

Given the large redshift range covered by our sample (see Figure 1), it is necessary to apply k-corrections to compute the X-ray rest-frame luminosities of our $70\mu\text{m}$ /X-ray galaxy sample. We assumed that the spectrum of our galaxies in X-ray follows a simple power law with photon index $\Gamma = 1.7$, and derived the ratio between rest-frame and observe-frame flux integration, to compute the intrinsic rest-frame flux density.

One of the main goals of our study is to explore the relationship between the galaxy host extinction and the central region obscuration. However, the neutral hydrogen column density identified in X-ray is integrated on the line-of-sight, therefore estimations of the intrinsic column density from X-ray spectrum fitting become model-dependent (Akylas et al. 2006). In order to simplify our analysis, we decided to use the hardness ratio (hereafter HR) as a good proxy of central region obscuration, define as:

$$HR = \frac{H - S}{H + S} \quad (3)$$

where H is X-ray hard band counts and S is X-ray soft band counts.

Our HR values are extracted from Brusa et al. (2010) for XMM observations and Elvis et al. (2009) for Chandra observations. To correct for the different observed bands between XMM

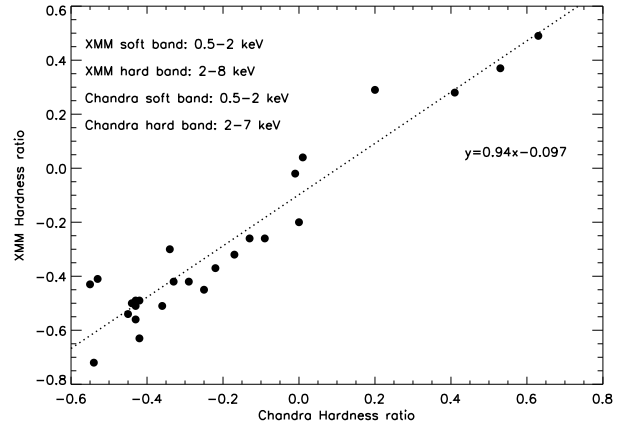


Figure 2. Hardness ratio extracted from the XMM catalog (Brusa et al. 2010) vs. value from the Chandra catalog (Elvis et al. 2009) for our 58 sources detected with both observatories. The different hard X-ray energy bands between the two observations, influence the hardness ratio measurements. We fit a simple line to estimate a conversion factor between the two different measurements. The fitted conversion factor is of 0.94 with small dispersion, consistent with the empirical expected value, predicted assuming a $\Gamma = 1.7$ X-ray power-law spectrum.

and Chandra, we assume once again that our source X-ray spectrum follows a power-law with $\Gamma = 1.7$. The final HR conversion factor from Chandra to XMM is ~ 0.94 . To validate our empirical conversion factor, we take advantage of our sources detected in both observatories. In Figure 2, we compared the HR from XMM with the HR from Chandra, for the overlapping detected sources. Just fitting a line between the HRs provides a similar conversion factor than our empirical estimation, proving the robustness of our conversion factor. Hereafter, all of our HR values are in XMM band system.

4 RESULTS

4.1 An AGN or star formation dominated sample?

Although our sample is drawn from both $70\mu\text{m}$ and X-ray catalogs, it is possible that the X-ray luminosity is attributed to a combination of emissions from supernovae remnant, high mass X-ray binaries (HMXBs), and low luminosity AGNs, instead of being generated by a single powerful AGN. For the low X-ray luminosity galaxies, it is difficult to identify the origin of X-ray emission. For instance, Arp220 is considered as the typical ULIRG dominated by star formation. However, the detection of high ionization Fe K lines in its X-ray spectrum prevents us from completely ruling out the possibility of a low luminosity AGN (Iwasawa et al. 2009).

Potentially, Ultraluminous X-ray sources (ULXs, X-ray point source; $L_X \geq 10^{39} \text{ erg s}^{-1}$) could explain the presence of X-ray emission in a star-forming galaxy. The presence of ULXs are mainly good indicators of recent star formation. However, deeper X-ray observations of Arp220 ruled out any ULX sources detection, in contradiction to the current scenario of recent starburst. A plausible interpretation is that ULXs may be embedded in dust, preventing them from being detected in X-ray survey (Smith et al. 2012).

In this paper, we still define Arp220 as a star-forming ULIRG, as it is commonly done in the literature. Also, we are using Mrk231

as an archetype for AGN ULIRG, as indicated by its strong X-ray emission.

4.1.1 AGN criterion from color-color selection

Mid-infrared IRAC color-color selection described by Stern et al. (2005, hereafter S05) is widely accepted as a robust method to select the AGN candidates. Such color criteria are efficient to separate AGN candidates from star-forming galaxies, due to the red $[3.6\mu\text{m}] - [4.5\mu\text{m}]$ color inferred by the combination of the power law continuum spectrum of the AGN and the relative weakness of the stellar bump feature at $1.6\mu\text{m}$ usually emitted by the host galaxy. Lacy et al. (2004) proposed another AGN diagnosis using a different IRAC color-color selection from S05. However, Choi et al. (2011) used complete AGN samples, based on the different selections (e.g. BPT diagram, $[\text{O III}]/\text{H}\beta$ ratio, high excitation line $[\text{Ne V}]$, and broad line region feature), to show that the S05 color-color selection is more robust than Lacy et al. (2004).

In Figure 3, we show the IRAC $[3.6\mu\text{m}]-[4.5\mu\text{m}]$ vs. $[5.8\mu\text{m}]-[8.0\mu\text{m}]$ color-color diagram of our $70\mu\text{m}/\text{X-ray}$ galaxies. The deep pink line indicates the AGN dominating region defined by S05. Using these criteria, we separated AGNs from our star-forming galaxies, LIRGs, and ULIRGs. Their estimated AGN fraction is 20% (4 out of 20; blue stars), 48% (29 out of 60; green square), and 92% (57 out of 62; red cross), respectively. There are 63.4% (90 out of 142) of $70\mu\text{m}/\text{X-ray}$ galaxies classified as AGN from the S05 selection criteria. We remark also that ULIRGs are overlapping more with AGN region in the diagram than the locus of star-forming galaxies; this result is consistent with literature that demonstrates an increasing infrared luminosity as the AGN fraction increases (Lee et al. 2010).

Our galaxy sample is spanning a wide range of redshifts which may influence the color-color properties due to k-correction effect. To better quantify this redshift effect, we placed the SED of Mrk231 and Arp220 in different redshifts, from $z = 0$ to $z = 3$, and monitored the color changes in Figure 3. Templates for Mrk231 and Arp220 are representative of AGN-dominated and star-forming dominated ULIRG, respectively. The Mrk231 colors never leave the S05 AGN region at any redshift because of its featureless power-law SED in mid-IR, while the Arp220 colors do not follow the S05 AGN criteria because that the different PAH emission lines entering into the IRAC photometry bands. The S05 criteria are therefore not extremely robust against Arp220-like star formation dominating ULIRG.

4.1.2 L_X vs. L_{IR} relation

The relation between hard X-ray luminosity and total infrared luminosity provides us with another method to determine whether star formation from host galaxy or AGN predominates the overall SED. While color-color selection can be altered by the presence of specific lines (Donley et al. 2008), total infrared luminosity is more robust because it is derived from $8\text{--}1000\mu\text{m}$ continuum (Smail et al. 2011).

In Figure 4 we display the hard X-ray ($2\text{--}10\text{keV}$) luminosity against total ($8\text{--}1000\mu\text{m}$) infrared luminosity for our $70\mu\text{m}/\text{X-ray}$ galaxies, according to their L_{IR} luminosity, subdivided into three sub-samples: star-forming galaxies, LIRGs, and ULIRGs (same symbols as in Figure 3). The X-ray luminosity versus Infrared luminosity plot shows a tight correlation with Spearman's $\rho \sim 0.88$. However, this strong correlation may be a mani-

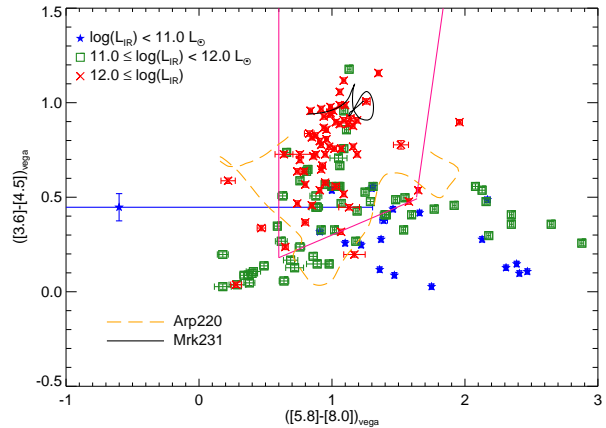


Figure 3. $[3.6]-[4.5]$ versus $[5.8]-[8.0]$ color-color diagram of $70\mu\text{m}$ galaxies with X-ray detection. The different L_{IR} -selected galaxy sample follow the description of Figure 1, with blue stars, green squares and red cross indicating star-forming galaxies, LIRGs and ULIRGs respectively. The pink solid continuous line represents the boundaries of the AGN region defined by Stern et al. (2005). Orange dash line and black solid line represent the evolution with redshift from $z = 0$ to $z = 3$ of the colors of Arp220 and Mrk231 templates, respectively. The S05 criterion are not efficient in separating AGNs and Arp220-like star-forming dominated ULIRGs.

festation of an observational bias. To confirm this, we need to estimate the upper and lower limits in the L_X vs. L_{IR} plot. In the case of the total infrared luminosity, we slice the whole $70\mu\text{m}$ catalog (Kartaltepe et al. 2010) into several redshift bins from $z = 0.5$ to $z = 3$, and identify the maximum and minimum total infrared luminosity. For the hard X-ray luminosity, we simulate the lower X-ray luminosity in the same redshift bins using the Chandra flux limits, and measure the upper X-ray luminosity directly from the XMM catalog (Brusa et al. 2010). The results are displayed as gray regions in Figure 4. These observational limits and their evolution with redshift indeed explain the tight correlation between the infrared and X-ray luminosities. A deeper (and less extended) X-ray survey from 4 Ms Chandra Deep Field South (CDFs) has demonstrated that some X-ray faint sources with bright total infrared luminosity are indeed missing from our shallower X-ray observations (Mullaney et al. 2012).

By studying X-ray properties of star-forming galaxies, Ranalli et al. (2003) demonstrated that hard X-ray luminosity is proportional to star formation rate (SFR). In fact, the most important contributors of X-ray emission in such galaxies are the high mass X-ray binaries (HMXBs). Franceschini et al. (2003) explored the X-ray properties of a sample of ULIRGs without AGN signature. The conclusion of their work is that the X-ray luminosity and spectral shape of most ULIRGs are dominated by hot thermal plasma and X-ray binaries, originated in recent starburst region.

On the other hand, because of the presence of the parsec-scale dust “torus” surrounding the accretion disk of the central SMBHs, AGNs can also emit light in the infrared wavelength (Gandhi et al. 2009). Indeed, the ultraviolet and optical light emit by the central accretion disk is absorbed by the dust and reemit in infrared. Gandhi et al. (2009) observed the core of nearby AGNs with unprecedented high spatial resolutions in both mid-IR and X-ray wavelength, demonstrated a strong correlation between $12.3\mu\text{m}$ and hard X-ray luminosities. These observations unambiguously demonstrated the existence of AGN drive mid-IR emission without contamination from the host galaxy. Based on the intrinsic

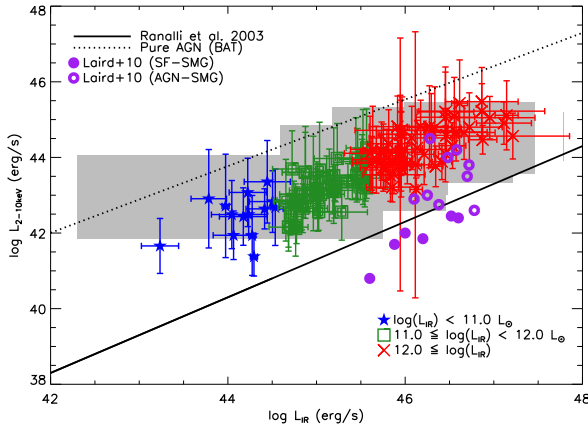


Figure 4. X-ray luminosity versus total infrared luminosity of 70 μ m selected galaxies with X-ray detection. Symbols are the same than in Figure 3. The X-ray luminosity error bars are derived from the estimated flux errors and the total infrared luminosity error bars are derived from the 1σ probability distribution of the χ^2 SED fitting. Gray regions represent the areas covered by maximum and minimum luminosities in different redshifts bins drawn from the full X-ray selected and 70 μ m selected samples. These observational limitations are inducing the apparent strong correlation between L_X and L_{IR} observed in the COSMOS field. Black dot line and black solid line represent the L_X vs L_{IR} relations for pure AGN and star-forming galaxy samples respectively (Mullaney et al. 2011; Ranalli et al. 2003). The luminosities of star-forming submillimeter galaxies (SMGs) and AGN SMGs, based on their X-ray spectrum fitting, are represented by filled and open purple circles respectively (Laird et al. 2010). Although 70 μ m/X-ray galaxies suffer large contamination from star formation, their location in this L_X vs L_{IR} diagram is consistent with this of AGN dominated SMGs.

AGN/quasar IR SED from Netzer et al. (2007), Mullaney et al. (2011) related the 12.3 μ m luminosity to the total infrared luminosity (L_{IR}) (their equation 5). By combining the Gandhi et al. (2009) and Mullaney et al. (2011) relations, we derived the unbiased L_X vs. L_{IR} relation for AGNs, free of any contamination from the host galaxy. This “pure” AGN L_X vs. L_{IR} relation is represented by the dotted line in Figure 4. Such relation has been confirmed by Swift-BAT X-ray selected AGN population (Tueller et al. 2010), together with IRAS infrared measurements (BAT/IRAS AGN). Indeed, their 60 μ m luminosity is more likely powered by the AGN rather than star formation activity from the host galaxy because of linearly increasing correlation between L_{IR} and L_X (Mullaney et al. 2012). For our COSMOS sample, the L_X vs. L_{IR} distribution of 70 μ m/X-ray galaxies deviates from AGN relation and star-forming relation by 0.5 – 1 dex and 1 – 2 dex, respectively. From the infrared and X-ray continuum perspective, AGNs approximately dominate the entire system.

Submillimeter galaxies (SMGs) are a population of objects selected according to their detection in submillimeter wavelengths. This population is dominated by strongly star-forming galaxies at high redshift, with this star formation producing a large amount of cold dust (Chapman et al. 2005). The concomitance in redshifts and infrared luminosities with ULIRGs indicates that SMGs may be an early stage of evolution of the merger scenario (Greve et al. 2005; Biggs & Ivison 2008; Engel et al. 2010). Ultra-deep X-ray observations for those distant star-forming galaxies indicate that 20-30% of SMGs host an AGN (Alexander et al. 2005). Laird et al. (2010) have studied the X-ray spectral properties of SMGs to classify them as AGN or starburst. These objects are represented in Figure 4

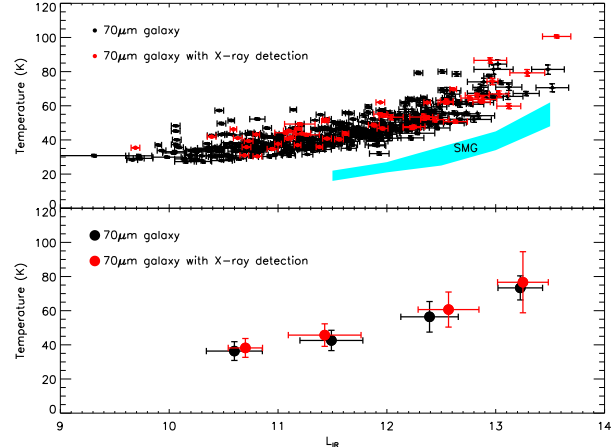


Figure 5. *Upper panel* : Luminosity-Temperature diagram; black points and red points refer to all 70 μ m galaxies and 70 μ m/X-ray galaxies, with temperatures derived from a single black-body fit with fixed emissivity. Both total infrared luminosity and temperature error bars are estimated from the 1σ probability distribution of the χ^2 SED fitting. Temperatures depend strongly of redshift, given it was estimated from one photometric band only, which result in warmer temperatures at higher redshifts. Similar effects are observed with the SMG population, whose luminosity-temperature relation is shown as the cyan area, although they have typically lower dust temperature for similar infrared luminosity (Chapman et al. 2005). *Lower panel* : Average temperature for different bins of total infrared luminosity (average from the values of upper panel) in different total infrared luminosity interval; black points and red points refer to all 70 μ m galaxies and 70 μ m/X-ray galaxies. The presence of AGN does not enhance the dust temperature of 70 μ m-selected galaxies.

with open and closed purple circles, respectively. Our 70 μ m/X-ray galaxies appear to share the same L_X vs. L_{IR} relation as the AGN-dominated SMGs.

In summary, all indicators in the L_X vs. L_{IR} distribution of our 70 μ m/X-ray galaxies converge toward a AGN dominated population.

4.2 Dust temperature of host galaxy

According to the predictions from the merger scenario, galaxy interaction triggers massive star formation, generating large amount of dust, at the same time, it disturbs the gas distribution, funneling it toward the central black hole, feeding the accretion disk, and therefore generating a phase of nuclear activity (Imanishi et al. 2010). If the center of the galaxy harbors an AGN, dust in host galaxy could be influenced by the radiations produced by the nucleus. One way to trace radiative feedback from AGN, is to observe the galaxy in the far-infrared wavelengths, as they are a good tracer of the dust temperature in the host galaxy (Magdis et al. 2010).

In order to accurately determine the wavelength at the peak of blackbody radiation, and separate several cold dust components with different temperatures, information on the fluxes in the Rayleigh-Jeans tail of the blackbody, hence at longer wavelength, is essential. However, in a simple case, assuming a single blackbody profile with fixed emissivity $\beta = 1.5$ in the Rayleigh-Jeans regime, $F_{70\mu m}$ and $F_{160\mu m}$ fluxes are sufficient enough to fit Wien regime of the blackbody. In this simplified case, we can derive the upper limit of dust temperature from the limited information (for details of the calculation, see section 3.3).

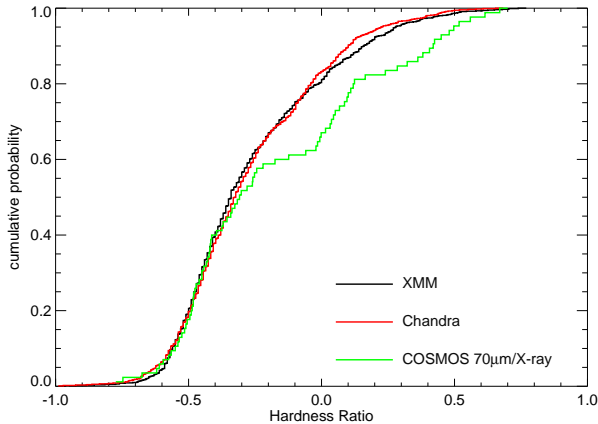


Figure 6. Kolmogorov-Smirnov test: the hardness ratio cumulative probability distribution of XMM, Chandra, and $70\mu\text{m}/\text{X-ray}$ selected galaxy samples represented in black, red, and green color lines respectively. Distribution of XMM and Chandra indicates these samples are drawn from the same population. However $70\mu\text{m}/\text{X-ray}$ galaxies seems not drawn from the same population than purely X-ray selected samples. The distribution indicates an excess of HR at ≥ -0.3 , revealing that the cold dust from the host starburst galaxy may be responsible of additional obscuration.

As shown in Figure 5, the dust temperature of $70\mu\text{m}$ galaxies correlates strongly with the total infrared luminosity. This is actually an observational bias because of a monochromatic wavelength for estimating the dust temperature. Indeed, at higher redshifts, the rest-frame flux corresponds to shorter wavelengths, and therefore probes warmer temperature. A similar incompleteness bias is acting on the estimation of dust temperature for SMGs, the selection at longer wavelengths (observed frame $850\mu\text{m}$, i.e. $\sim 300\mu\text{m}$ at $z \sim 2$) probed a lower dust temperature regime (Chapman et al. 2005).

However, incomplete bias have little influence in our comparative study between $70\mu\text{m}$ -selected with and without X-ray detection. In total, we have estimated the temperature for 463/1503 (31%) of the $70\mu\text{m}$ -selected galaxies, of which 52/142 (37%) with X-ray detection. Such a large sample of $70\mu\text{m}$ galaxies with/without X-ray provides a good statistical ground to investigate any difference in dust temperature between AGN and non-AGN galaxies.

In Figure 5, $70\mu\text{m}$ galaxies with/without X-ray detection are labeled as red/black filled circles, respectively, with the error bars estimated from the 1σ probability distribution of χ^2 fit. Although $70\mu\text{m}/\text{X-ray}$ galaxies display systematically slightly higher dust temperature compare to non-X-ray detected $70\mu\text{m}$ galaxies (a shift of $1.85\text{--}4.25\text{K}$ for a temperature of $36.3\text{--}73.3\text{K}$), the difference is not significant given the large uncertainties in the measurements (between 5.50K and 17.88K). Therefore, we do not observe any noticeable effects of the presence of AGN on the dust temperature of the host galaxy, in agreement with the recent observations based on Herschel far-infrared result from Elbaz et al. (2010).

4.3 Hardness ratio of $70\mu\text{m}/\text{X-ray}$ galaxies

To explain the diversity of AGNs (e.g., narrow-lines vs. broad-lines), a unified model, based on the variation of obscuration due to the orientation of the dust torus surrounding the SMBH accretion disk, has been proposed. In such model, the presence of an

edge-on dust torus not only blocks the broad-line emissions, but also increases the absorption in soft X-ray because of the higher hydrogen column density (Antonucci 1993).

In addition, for on-going galaxy mergers, the triggered star formation and higher dust production generate a higher neutral hydrogen column density as well, absorbing soft X-ray (e.g., Esquej et al. 2012). Indeed, using the Extended Chandra Deep Field-South (ECDF-S) dataset, Treister et al. (2009) observed large obscuration of the soft X-ray emission in star-forming galaxies hosting an AGN at high redshifts, revealing a large amount of neutral hydrogen density on the line-of-sight.

We like to investigate if there is a direct connection between the obscuration properties of the AGN and those of the host galaxy. As absorption affects the soft X-ray emissions more than the hard X-ray emissions, the HR is a good tracer of obscuration, with higher value of HR corresponding to larger absorption. To test whether our two samples, X-ray selected galaxies and $70\mu\text{m}/\text{X-ray}$ galaxies, are consistent with being drawn from the same sample (i.e. our null hypothesis), we apply Kolmogorov-Smirnov (K-S) test (*Numerical Recipes*, Press et al. 1992).

As an initial test, we examined the HR of XMM and Chandra X-ray selected sources, to test the robustness of our conversion between XMM HR and Chandra HR (for details, see section 3.4). The results of our K-S test for these populations are shown in Figure 6, with the HR cumulative probability distribution of XMM selected sample in black and Chandra selected sample in red, and the K-S parameters are summarized in Table 3. Our result is consistent with XMM and Chandra selected samples being drawn from the same population. Although two X-ray facilities have different sky coverage and depth, XMM HR distribution is identical to the Chandra HR distribution.

Then, we apply the K-S test between the $70\mu\text{m}/\text{X-ray}$ and XMM samples. This time, the null hypothesis is rejected at a significance of 99% confidence level, implying that $70\mu\text{m}/\text{X-ray}$ galaxies and XMM galaxies are drawn from different populations. The K-S test between $70\mu\text{m}/\text{X-ray}$ and Chandra selected samples also rejects the hypothesis. Figure 6 displays the cumulative probability distribution of HR from XMM (black solid line), Chandra (red solid line), and $70\mu\text{m}/\text{X-ray}$ (green solid line) selected samples. The K-S parameters resulting from the three tests are summarized in Table 3.

The tests indicate that $70\mu\text{m}/\text{X-ray}$ galaxies include more obscured AGNs than purely X-ray selected samples. This implies that, in the case of AGNs hosted by dust enshrouded galaxies, the presence of an additional physical process not accounted in the AGN unified model scheme. We speculate that the excess of obscuration is not only attributed to absorption on the line-of-sight by continuum or clumpy dust torus around the SMBH, but also is associated with an additional more diffuse dust component generated by strong star formation in the host galaxy. The starburst can be subsequent of an event involving the whole system (e.g. merger) or generated by the circumnuclear region (e.g. bar). That is to say, AGN is hosted by a galaxy, hence we can not neglect the influence of the host galaxy on AGN properties. Only X-ray observations with very high spatial resolution will enable us to identify the origin of the extra amount of neutral hydrogen.

Table 3. Results of the K-S test on the hardness ratio between different catalogs

Catalogs	D_{\max}	Significant level	Hypothesis
XMM & Chandra	0.0397	0.466	Not Reject
XMM & 70 μ m/X-ray	0.1918	0.0054	Reject
Chandra & 70 μ m/X-ray	0.2105	0.0017	Reject

5 DISSUSSION

5.1 AGN influence on the host galaxy dust temperature?

Our analysis in section 4.2 demonstrates that we have no strong evidence of any influence by AGN on the host galaxy dust temperature. Although our result is in agreement with recent result (e.g. Elbaz et al. 2010), it is in contradiction with the recent work by Rafferty et al. (2011).

Using infrared color $\log(F_{24\mu\text{m}}/F_{70\mu\text{m}})$, to sample the blackbody temperature profile, Rafferty et al. (2011) concluded that galaxies hosting an AGN present a high dust temperature. We reproduced their analysis for our sample, as shown in Figure 7. The 70 μ m/X-ray galaxies present a higher color index in average than overall 70 μ m galaxies at all redshifts, a similar conclusion to Rafferty et al. (2011). Though the 70 μ m/X-ray galaxies show higher $\log(F_{24\mu\text{m}}/F_{70\mu\text{m}})$, they still agree with the local definition of cold dust (de Grijs et al. 1985; Sanders et al. 1988b).

To explain the difference in color index, we looked at the evolution of the $F_{24\mu\text{m}}/F_{70\mu\text{m}}$ color as a function of the redshift for two typical objects, the star-forming ULIRG Arp220 and the AGN ULIRG Mrk231. We used the galaxy templates provided by Polletta et al. (2007), as shown in Figure 7. In the case of Arp220, the rest frame 9.7 μ m absorption line is shifted into the 24 μ m band at redshift $z \sim 1.5$, causing an apparent lower value of the color index. Similarly, at $z > 2$, the 7.7 and 8.2 μ m PAH emission lines are entering the 24 μ m band, inducing a higher $F_{24\mu\text{m}}/F_{70\mu\text{m}}$ color ratio. In the case of Mrk231, the AGN driven power-law continuum produces a more stable color index. Our 70 μ m/X-ray samples follow the same color index of Mrk231-like galaxies across the redshift range $0 < z < 3$, and the remaining parts of our samples follow more a Arp220-like profile. Therefore, the difference observed in $F_{24\mu\text{m}}/F_{70\mu\text{m}}$ color between the two samples has little to do with the average diffuse dust temperature.

To have a robust measurement of the variation of dust temperature in the host galaxy, we need to explore the longer wavelengths that have less perturbation from emission and absorption line features. For instance, measuring the longer wavelength color (e.g. $F_{70\mu\text{m}}/F_{160\mu\text{m}}$) is a more accurate method to estimate the dust temperature (Casey 2012). In order to simplify the temperature fitting, the models of temperature usually assume that β is a constant value. However, it depends on which photometric bands are included; shorter wavelength photometry will induce the lower β value, and probe a systematically higher temperature (Magnelli et al. 2012). Our fitting procedure provides no strong evidence that the cold dust of host galaxy is heated by AGN (see section 4.2). Such result is consistent with the latest work from the Herschel observations (Elbaz et al. 2010). Actually, the photometry in the 250 μ m, 350 μ m, and 500 μ m bands provides information on the Rayleigh-Jeans portion of the spectra, and therefore enables a more accurate estimation of the dust temperature of the host galaxy. Such precise measurements show a 2 – 3K difference between the dust temperature of a galaxy with AGN, and without

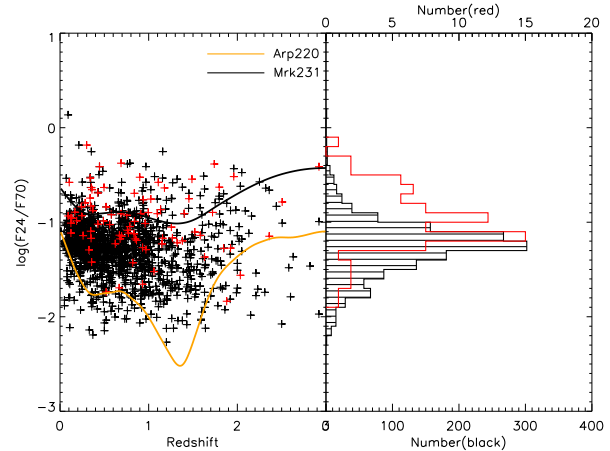


Figure 7. Distribution of $(F_{24\mu\text{m}}/F_{70\mu\text{m}})$ color index for 70 μ m selected sample and 70 μ m/X-ray sample. *Left panel* : Distribution of the color against redshift for the 70 μ m galaxies (black crosses) and the 70 μ m/X-ray sample (red crosses). The black and orange lines indicate the evolution of Mrk231 and Arp220 flux ratio as a function of redshift, computed using the templates from Polletta et al. (2007). *Right panel* : Histogram of the color index for 70 μ m-selected galaxies in black and 70 μ m/X-ray in red, with the red histogram normalized to the peak of black sample for better display (bottom and top axis represent the number of 70 μ m-selected galaxies and 70 μ m/X-ray respectively). The 70 μ m galaxies have a median color index of $\log(F_{24\mu\text{m}}/F_{70\mu\text{m}}) \sim -1.25$, while for 70 μ m/X-ray galaxies it is of ~ -0.99 . Both satisfy the local cold dust definition of $\log(F_{24\mu\text{m}}/F_{70\mu\text{m}}) \leq -0.7$ (de Grijs et al. 1985; Sanders et al. 1988b).

AGN (Elbaz et al. 2010). This implies that the far-infrared emission of the galaxy is dominated by the dust blackbody emission heated by star formation, in agreement with previous studies. As an example, Silverman et al. (2009) reached a similar conclusion from the optical zCOSMOS dataset. Using [O III]-corrected [O II] emission lines as star formation indicator, the correlation between SFR and X-ray luminosity, they demonstrated that there is ongoing star formation in galaxies hosting AGNs. With the exception of the warm dust component (as shown by the $F_{24\mu\text{m}}/F_{70\mu\text{m}}$ color), neither this work nor Silverman et al. (2009) seem to display any truncation of the star formation by AGN radiative feedback.

5.2 AGN obscuration from starburst?

According to the major merger scenario of galaxy evolution, developed to interpret a potential ULIRG-QSO connection, galaxies undergo an obscuration phase after the merger occurred due to an enhancement of star formation and dust production. This obscured phase is thought to be ended by a consecutive AGN phase, during which feedback from the central SMBH repels the dust (Hopkins et al. 2008). Giving an illustration, the NGC 6240 Seyfert galaxy is a well studied ULIRG, with high infrared luminosity indicating a starburst activity which generates a large amount of dust and molecular gas (Iono et al. 2007). A detailed X-ray spectrum from Chandra of NGC 6240 revealed a very strong absorption from the neutral gas column density N_H (Ptak et al. 2003). Thanks to the higher spatial resolution, Chandra observations of NGC 6240 identified the presence of a double AGNs system, hidden in the core of the galaxy (Komossa et al. 2003). These observations are consistent with the idea that galaxy was formed consequentially of a merger.

To efficiently investigate the evolutionary stages of the AGN

concomitance with star formation, our approach is to study the properties galaxies detected in both infrared and X-ray. Rafferty et al. (2011) had a similar approach to ours, looking for the X-ray counterpart of 70 μ m-selected galaxies in the ECDF-S and EGS fields. Performing both a X-ray spectrum and a X-ray band ratio analysis, assuming a power-law spectrum with different column densities, they did not identify any excess of neutral hydrogen in 70 μ m-selected X-ray sources compared to other X-ray selected AGNs. They concluded that the absence of obscured AGN among the star-forming galaxies contradicts to the current AGN and galaxy co-evolution model (Hopkins et al. 2008). Actually, the main reason why Rafferty et al. (2011) did not detect any additional obscured AGN from star-forming galaxies, is probably the statistical insufficiency of their sample. They only had accessed to 17 of AGN detected in 70 μ m, with hydrogen column density N_H derived by X-ray spectral analysis (Tozzi et al. 2006), comparing with whole AGN population.

In contrast, our large sample (142 70 μ m/X-ray galaxies) enables us a proper statistical study. We therefore took a different approach by applying a K-S test on the distribution of hardness ratio to investigate if 70 μ m/X-ray galaxies and X-ray selected AGNs are drawn from the same sample (see section 4.3). Trichas et al. (2009) attempted to conduct such study based on shallower 70 μ m observations from the Spitzer Wide Area Infrared Extragalactic (SWIRE) survey, but did not have sufficient statistics to conclude if 70 μ m galaxies with X-ray detection were different from the global X-ray population. However, owing to the deeper 70 μ m observations in the COSMOS field, we could extract a larger sample, and our K-S test shows in less than 1% of probability for 70 μ m galaxies with X-ray detection to be drawn from the global X-ray population. Such result is in agreement with the merger galaxy formation scenario: the neutral hydrogen obscuration in infrared-luminous AGN not only comes from the dust torus component around the AGN, but also from extreme star formation region in the host galaxy.

6 CONCLUSION

We have investigated the properties of 142 galaxies both detected in X-ray and 70 μ m in the COSMOS field. X-ray data are obtained from both XMM and Chandra point source catalogs, and 70 μ m photometry is drawn from Spitzer-MIPS 70 μ m point source catalog. We classified our sample into three distinct subsamples according to their respective total infrared luminosity (L_{IR}): star-forming galaxies ($L_{IR} < 10^{11} L_{\odot}$), luminous infrared galaxies (LIRGs, $10^{11} L_{\odot} \leq L_{IR} < 10^{12} L_{\odot}$), and ultra-luminous infrared galaxies (ULIRGs, $L_{IR} \geq 10^{12} L_{\odot}$), with median redshifts of $z \sim 0.168$, 0.518 and 1.268, respectively. The major conclusions for this study are as follows:

- (i) We applied two methods to determine which mechanism dominates the SED, star formation or AGN:
 - i) Using Spitzer-IRAC colors, we have shown that the majority of our sample is dominated by AGN. Although the higher AGN fraction accompanies with higher total infrared luminosity (L_{IR}), the presence of PAH emission lines related to star formation could disturb AGN identification.
 - ii) Using the relation between hard X-ray (2-10keV) and total infrared luminosity L_{IR} (8-1000 μ m), we found that our samples are dominated by AGN, with property comparable to AGN detected SMGs.
- (ii) We provided evidences for additional X-ray obscuration in X-ray detected 70 μ m galaxies, in agreement with current

AGN/starburst co-evolution model (Hopkins et al. 2008). A K-S test on the modified HR between 70 μ m/X-ray galaxies and whole X-ray samples rejected the assumption of them to be originated from the same population within 99% confidence level, supporting the idea that the excess of X-ray absorption does not come from the AGN dusty torus obscuration, but probably from additional diffuse obscuration generated by the star formation in the galaxy.

(iii) We estimated the dust temperature of our 70 μ m galaxy samples by fitting their far-infrared photometries with fixed emissivity models. Despite the presence of a warm dust component, the cold dust shows a similar temperature in host galaxy with and without AGN, indicating that the longer wavelengths are still dominated by star formation. This evidence conflicts with a scenario where radiative feedback from the AGN truncates the star formation in the host galaxy.

ACKNOWLEDGEMENTS

The work presented here is supported by the National Science Council of Taiwan under the grants NSC99-2112-M-003-002-MY2, NSC99-2119-M-003-005, and NSC 99-2112-M-003-001-MY2. We would like to acknowledge the wonderful work made by Jeyhan S. Kartaltepe on the Spitzer-COSMOS 70 μ m point source catalog on which our analyses are based. We would like to thank the following people for very useful discussions, suggestions, and comments: Lin-Wen Chen, Jeyhan S. Kartaltepe, Wei-Hao Wang, Albert Kong, Matthew A. Malkan, Nick Scoville, and David B. Sanders. This research used extensively the COSMOS survey archive data of the NASA/IPAC Infrared Science Archive, which is operated by the Jet Propulsion Laboratory, California Institute of Technology, under contract with the National Aeronautics and Space Administration.

REFERENCES

- Abazajian, K. N., Adelman-McCarthy, J. K., Agüeros, M. A., et al., 2009, *ApJS*, 182, 543
- Akylas, A., Georgantopoulos, I., Georgakakis, A., Kitsionas, S., & Hatziminaoglou, E., 2006, *A&A*, 459, 693
- Alexander, D. M., Smail, I., Bauer, F. E., et al., 2005, *Nature*, 434, 738
- Alonso-Herrero, A., Pérez-González, P. G., Alexander, D. M., et al., 2006, *ApJ*, 640, 167
- Antonucci, R., 1993, *ARA&A*, 31, 473
- Armus, L. 2006, *Astronomical Society of the Pacific Conference Series*, 357, 218
- Arnouts, S., Cristiani, S., Moscardini, L., Matarrese, S., Lucchin, F., et al., 1999, *MNRAS*, 310, 540
- Baan, W. A., Salzer, J. J., & Lewinter, R. D., 1998, *ApJ*, 509, 633
- Baldwin, J. A., Phillips, M. M., & Terlevich, R., 1981, *PASP*, 93, 5
- Bennert, N., Canalizo, G., Jungwiert, B., et al., 2008, *ApJ*, 677, 846
- Biggs, A. D., & Ivison, R. J., 2008, *MNRAS*, 385, 893
- Boquien, M., Bendo, G., Calzetti, D., et al., 2010, *ApJ*, 713, 626
- Borne, K. D., Bushouse, H., Lucas, R. A., & Colina, L., 2000, *ApJ*, 529, L77
- Braitto, V., Della Ceca, R., Piconcelli, E., et al., 2004, *A&A*, 420, 79
- Brand, K., Dey, A., Weedman, D., et al., 2006, *ApJ*, 644, 143

- Brusa, M., Civano, F., Comastri, A., et al., 2010, *ApJ*, 716, 348
- Canalizo, G., & Stockton, A., 2001, *ApJ*, 555, 719
- Capak, P., Aussel, H., Ajiki, M., et al., 2007, *ApJS*, 172, 99
- Cappelluti, N., Brusa, M., Hasinger, G., et al., 2009, *A&A*, 497, 635
- Casey, C. M., Chapman, S. C., Beswick, R. J., et al., 2009, *MNRAS*, 399, 121
- Casey, C. M., 2012, *MNRAS*, 425, 3094
- Chapman, S. C., Blain, A. W., Smail, I., & Ivison, R. J., 2005, *ApJ*, 622, 772
- Choi, P. I., Yan, L., Helou, G., et al., 2011, *ApJ*, 732, 21
- Clements, D. L., Dunne, L., & Eales, S., 2010, *MNRAS*, 403, 274
- Cui, J., Xia, X.-Y., Deng, Z.-G., Mao, S., & Zou, Z.-L., 2001, *AJ*, 122, 63
- de Grijp, M. H. K., Miley, G. K., Lub, J., & de Jong, T., 1985, *Nature*, 314, 240
- Donley, J. L., Rieke, G. H., Pérez-González, P. G., Rigby, J. R., & Alonso-Herrero, A., 2007, *ApJ*, 660, 167
- Donley, J. L., Rieke, G. H., Pérez-González, P. G., & Barro, G., 2008, *ApJ*, 687, 111
- Elbaz, D., Hwang, H. S., Magnelli, B., et al., 2010, *A&A*, 518, L29
- Elvis, M., Civano, F., Vignali, C., et al., 2009, *ApJS*, 184, 158
- Engel, H., Tacconi, L. J., Davies, R. I., et al., 2010, *ApJ*, 724, 233
- Esquej, P., Alonso-Herrero, A., Pérez-García, A. M., et al., 2012, *MNRAS*, 423, 185
- Franceschini, A., Braitto, V., Persic, M., et al., 2003, *MNRAS*, 343, 1181
- Farrah, D., Afonso, J., Efstathiou, A., et al., 2003, *MNRAS*, 343, 585
- Frazer, D. T., Sanders, D. B., Surace, J. A., et al., 2009, *AJ*, 138, 1261
- Gandhi, P., Horst, H., Smette, A., et al., 2009, *A&A*, 502, 457
- Greve, T. R., Bertoldi, F., Smail, I., et al., 2005, *MNRAS*, 359, 1165
- Haardt, F., & Maraschi, L., 1993, *ApJ*, 413, 507
- Hopkins, P. F., Hernquist, L., Cox, T. J., & Kereš, D., 2008, *ApJS*, 175, 356
- Hasinger, G., Cappelluti, N., Brunner, H., et al., 2007, *ApJS*, 172, 29
- Ilbert, O., Arnouts, S., McCracken, H. J., Bolzonella, M., Bertin, E., et al., 2006, *A&A*, 457, 841
- Ilbert, O., Capak, P., Salvato, M., et al., 2009, *ApJ*, 690, 1236
- Imanishi, M., Maiolino, R., & Nakagawa, T., 2010, *ApJ*, 709, 801
- Iono, D., Wilson, C. D., Takakuwa, S., et al., 2007, *ApJ*, 659, 283
- Iwasawa, K., Sanders, D. B., Evans, A. S., et al., 2009, *ApJ*, 695, L103
- Kartaltepe, J. S., Sanders, D. B., Le Floc'h, E., et al., 2010, *ApJ*, 709, 572
- Kartaltepe, J. S., Dickinson, M., Alexander, D. M., et al., 2012, *ApJ*, 757, 23
- Kocevski, D. D., Faber, S. M., Mozena, M., et al., 2012, *ApJ*, 744, 148
- Koekemoer, A. M., Aussel, H., Calzetti, D., et al., 2007, *ApJS*, 172, 196
- Komossa, S., Burwitz, V., Hasinger, G., et al., 2003, *ApJ*, 582, L15
- Kormendy, J., & Richstone, D., 1995, *ARA&A*, 33, 581
- Kovács, A., Chapman, S. C., Dowell, C. D., et al., 2006, *ApJ*, 650, 592
- Lacy, M., Storrie-Lombardi, L. J., Sajina, A., et al., 2004, *ApJS*, 154, 166
- Laird, E. S., Nandra, K., Pope, A., & Scott, D., 2010, *MNRAS*, 401, 2763
- Lee, N., Le Floc'h, E., Sanders, D. B., et al., 2010, *ApJ*, 717, 175
- Le Floc'h, E., Aussel, H., Ilbert, O., et al., 2009, *ApJ*, 703, 222
- Lehmer, B. D., Alexander, D. M., Bauer, F. E., et al., 2010, *ApJ*, 724, 559
- Levenson, N. A., Sirocky, M. M., Hao, L., et al., 2007, *ApJ*, 654, L45
- Lilly, S. J., Le Fèvre, O., Renzini, A., et al., 2007, *ApJS*, 172, 70
- Lilly, S. J., Le Brun, V., Maier, C., et al., 2009, *ApJS*, 184, 218
- Magdis, G. E., Elbaz, D., Hwang, H. S., et al., 2010, *MNRAS*, 409, 22
- Magdis, G. E., Daddi, E., Elbaz, D., et al., 2011, *ApJ*, 740, L15
- Magnelli, B., Lutz, D., Santini, P., et al., 2012, *A&A*, 539, A155
- Magorrian, J., Tremaine, S., Richstone, D., et al., 1998, *AJ*, 115, 2285
- Mullaney, J. R., Alexander, D. M., Goulding, A. D., & Hickox, R. C., 2011, *MNRAS*, 414, 1082
- Mullaney, J. R., Pannella, M., Daddi, E., et al., 2012, *MNRAS*, 419, 95
- Netzer, H., Lutz, D., Schweitzer, M., et al., 2007, *ApJ*, 666, 806
- Patel, H., Clements, D. L., Rowan-Robinson, M., & Vaccari, M., 2011, *MNRAS*, 415, 1738
- Polletta, M., Tajer, M., Maraschi, L., et al., 2007, *ApJ*, 663, 81
- Pozzi, F., Vignali, C., Gruppioni, C., et al., 2012, *MNRAS*, 423, 1909
- Prescott, M. K. M., Impey, C. D., Cool, R. J., & Scoville, N. Z., 2006, *ApJ*, 644, 100
- Press, W. H., Flannery, B. P., Teukolsky, S. A., & Vetterling, W. T., 1992, *Numerical Recipes*, 2nd edition (1992), Chapter 14
- Ptak, A., Heckman, T., Levenson, N. A., Weaver, K., & Strickland, D., 2003, *ApJ*, 592, 782
- Rafferty, D. A., Brandt, W. N., Alexander, D. M., et al., 2011, *ApJ*, 742, 3
- Ranalli, P., Comastri, A., & Setti, G., 2003, *A&A*, 399, 39
- Salvato, M., Hasinger, G., Ilbert, O., et al., 2009, *ApJ*, 690, 1250
- Sanders, D. B., Soifer, B. T., Elias, J. H., et al., 1988, *ApJ*, 325, 74
- Sanders, D. B., Soifer, B. T., Elias, J. H., Neugebauer, G., & Matthews, K., 1988, *ApJ*, 328, L35
- Sanders, D. B., Phinney, E. S., Neugebauer, G., Soifer, B. T., & Matthews, K., 1989, *ApJ*, 347, 29
- Sanders, D. B., & Mirabel, I. F., 1996, *ARA&A*, 34, 749
- Sanders, D. B., Salvato, M., Aussel, H., et al., 2007, *ApJS*, 172, 86
- Scoville, N., Aussel, H., Brusa, M., et al., 2007, *ApJS*, 172, 1
- Scoville, N., Abraham, R. G., Aussel, H., et al., 2007, *ApJS*, 172, 38
- Scott, K. S., Austermann, J. E., Perera, T. A., et al., 2008, *MNRAS*, 385, 2225
- Shi, Y., Rieke, G., Lotz, J., & Perez-Gonzalez, P. G., 2009, *ApJ*, 697, 1764
- Silverman, J. D., Lamareille, F., Maier, C., et al., 2009, *ApJ*, 696, 396
- Smail, I., Swinbank, A. M., Ivison, R. J., & Ibar, E., 2011, *MNRAS*, 414, L95
- Smith, B. J., Swartz, D. A., Miller, O., et al., 2012, *AJ*, 143, 144
- Stern, D., Eisenhardt, P., Gorjian, V., et al., 2005, *ApJ*, 631, 163
- Symeonidis, M., Rosario, D., Georgakakis, A., et al., 2010, *MNRAS*, 403, 1474
- Symeonidis, M., Georgakakis, A., Seymour, N., et al., 2011, *MNRAS*, 417, 2239

- Tozzi, P., Gilli, R., Mainieri, V., et al., 2006, *A&A*, 451, 457
- Treister, E., Cardamone, C. N., Schawinski, K., et al., 2009, *ApJ*, 706, 535
- Treister, E., Natarajan, P., Sanders, D. B., et al., 2010, *Science*, 328, 600
- Trichas, M., Georgakakis, A., Rowan-Robinson, M., et al., 2009, *MNRAS*, 399, 663
- Trump, J. R., Impey, C. D., McCarthy, P. J., et al., 2007, *ApJS*, 172, 383
- Tueller, J., Baumgartner, W. H., Markwardt, C. B., et al., 2010, *ApJS*, 186, 378
- van der Werf, P. P., Isaak, K. G., Meijerink, R., et al., 2010, *A&A*, 518, L42
- Veilleux, S., Kim, D.-C., & Sanders, D. B., 2002, *ApJS*, 143, 315
- Veilleux, S., Rupke, D. S. N., Kim, D.-C., et al., 2009, *ApJS*, 182, 62
- Voit, G. M., 1992, *MNRAS*, 258, 841
- Walton, D. J., Roberts, T. P., Mateos, S., & Heard, V., 2011, *MNRAS*, 416, 1844
- Yang, M., Greve, T. R., Dowell, C. D., & Borys, C., 2007, *ApJ*, 660, 1198
- Yuan, T.-T., Kewley, L. J., & Sanders, D. B., 2010, *ApJ*, 709, 884